Science of the Total Environment 633 (2018) 1571–1578

Contents lists available at ScienceDirect

Science of the Total Environment

journal homepage: www.elsevier.com/locate/scitotenv

Dual carbon isotopes (^{14}C and ^{13}C) and optical properties of WSOC and HULIS-C during winter in Guangzhou, China

Junwen Liu [a], Yangzhi Mo [b], Ping Ding [b], Jun Li [b,*], Chengde Shen [b], Gan Zhang [b]

[a] Institute for Environmental and Climate Research, Jinan University, Guangzhou, China
[b] State Key Laboratory of Organic Geochemistry, State Key Laboratory of Isotope Geochemistry, Guangzhou Institute of Geochemistry, Chinese Academy of Sciences, Guangzhou, China

HIGHLIGHTS

- Dual carbon isotopes (^{14}C and ^{13}C) of WSOC and HULIS-C were measured in Guangzhou, China.
- Two-thirds of WSOC and HULISC-C mass were derived from biomass with the rest from fossil fuel.
- Fossil and non-fossil sources contributed 10% and 80% to the light absorption of BrC.

GRAPHICAL ABSTRACT

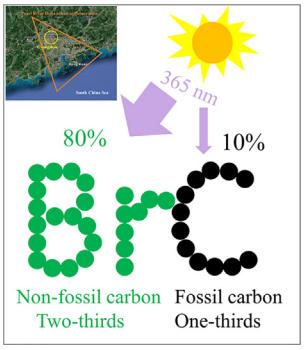

ARTICLE INFO

Article history:
Received 21 February 2018
Received in revised form 23 March 2018
Accepted 24 March 2018
Available online 4 April 2018

Editor: Xinbing Fen

Keywords:
Brown carbon
Humic-like substance
Light absorption
Radiocarbon
Water-soluble organic carbon

ABSTRACT

Water-soluble brown carbon (ws-BrC) exerts an important influence on climate change, but its emission sources and optical properties remain poorly understood. In this study, we isolated two ws-BrC proxies, water-soluble organic carbon (WSOC) and humic-like substance carbon (HULIS-C), from particulate matter collected in Guangzhou, China, during December 2012 for the measurement of dual carbon isotopes (^{14}C and ^{13}C) and light absorption. The mass absorption efficiencies of WSOC and HULIS-C at 365 nm were 0.81 ± 0.16 and 1.33 ± 0.21 $m^2\ g^{-1}$ C, respectively. The ^{14}C results showed that two-thirds of WSOC and HULIS-C were derived from non-fossil sources (e.g., biomass burning and biogenic emission), and the remaining third was derived from fossil sources. The $\delta^{13}C$ values of WSOC and HULIS-C were −23.7 ± 1.2‰ and −24.2 ± 0.9‰, respectively, underlining the limited influences of C4 plants and natural gas on ws-BrC. Fitting the data to a multiple linear regression, we further concluded that approximately 80% and 10% of the light absorption at 365 nm was due to non-fossil and fossil carbon, respectively. Non-fossil sources of ws-BrC, such as the burning of agricultural residue, were responsible for the light absorption recorded in Guangzhou.

© 2018 Elsevier B.V. All rights reserved.

1. Introduction

Organic carbon (OC) aerosols are ubiquitous and have profound effects on air quality, the radiation budget, and climate change (Kanakidou et al., 2005; Kulmala et al., 2011). In most climate models, OC is currently simply treated as a driver of cooling in the atmosphere (Bond et al., 2011; Ma et al., 2012) due to the widespread belief that black carbon (BC or elemental carbon, EC) and mineral dust are the only two important light-absorbing components of the atmosphere. However, there is an increasing body of evidence suggesting that one type of OC, i.e., brown carbon (BrC), can absorb solar radiation

* Corresponding author at: 511, Kehua Street, Tianhe, Guangzhou, China.
E-mail address: junli@gig.ac.cn. (J. Li).

https://doi.org/10.1016/j.scitotenv.2018.03.293
0048-9697/© 2018 Elsevier B.V. All rights reserved.

efficiently in the near-UV and visible ranges, and it is therefore thought to be an important contributor to regional and global radiative forcing (Andreae and Gelencsér, 2006; Alexander et al., 2008; Feng et al., 2013; Laskin et al., 2015; Liu et al., 2015). It is estimated that at the global scale the radiative forcing of BrC ranges from +0.22 to +0.57 W/m^2, accounting for 27–70% of BC forcing (Lin et al., 2014a).

Unfortunately, the emission sources and optical properties of BrC, which are required for modelling its climate effects, are poorly understood. Laboratory experiments have shown that BrC sources are analogous to those of OC, including biomass burning (BB; e.g., wood, grass, and crop straw) (Chen and Bond, 2010; Du et al., 2014; Olson et al., 2015), fossil fuel combustion (e.g., coal and petroleum) (Bond, 2001; Du et al., 2014; Olson et al., 2015; Sun et al., 2017), and atmospheric reactions (e.g., oxidation of gaseous precursors and the process of atmospheric aging) (Lin et al., 2014b). In the real atmosphere, BB is thought to be the dominant source of BrC (Chen and Bond, 2010; Arola et al., 2011; Feng et al., 2013; Washenfelder et al., 2015; Lin et al., 2017), although some studies have indicated that fossil-fuel-combustion related activities such as traffic exhaust in the USA (Hecobian et al., 2010; Zhang et al., 2013) and coal combustion in north China (Yan et al., 2017) can also release a large amount of BrC aerosols. The influence of emission sources on determining the light absorption coefficients of BrC is ambiguous. Chamber experiments have shown that the absorptivity of BB-derived BrC depends on the burning conditions but not the biomass type (Saleh et al., 2014), although the absorptivity of fossil-fuel-derived BrC is seemingly significantly influenced by fuel type. For example, Du et al. (2014) found that the light absorptivity of BrC emitted by a gasoline motorcycle was ~6 times lower than that of BrC emitted by a diesel tractor. These observations indicate that BrC mass loading and light absorptivity in the real atmosphere are not predominately controlled by one single source. Therefore, identifying the relative contribution of emission sources to light absorption by BrC aerosols, especially in regions with intensive anthropogenic activities such as China, is crucial and is urgently needed to improve predictions of the climate forcing effects of aerosols.

Guangzhou is geographically located at the core position of the Pearl River Delta (PRD) and is the third-largest megacity in China, with a population of >10 million. Although the levels of carbonaceous aerosols and air pollution in the PRD have been the subject of intense discussions for decades (e.g., Cao et al., 2003; Deng et al., 2008; Lai et al., 2016), few BrC-related studies have been conducted in this key area. Using a three-wavelength photo-acoustic soot spectrometer (PASS-3) and aerosol mass spectrometer (AMS), Yuan et al. (2016) explored the optical properties of BrC in the PRD and found that it contributed ~6–12% and ~4–10% of the total light absorption at 405 nm and 532 nm, respectively. A slightly lower light absorption at 532 nm (~3%) for BrC was reported by Lan et al. (2017). Because optical instruments cannot chemically separate BrC from other components for further analysis, filter-based samples are frequently prepared by solvent extraction and the corresponding extracts, such as water-soluble organic carbon (WSOC), can be used as surrogates (Cheng et al., 2011; Kirillova et al., 2016) of water-soluble BrC (ws-BrC). Recently, Huang et al. (2016) measured the optical properties of WSOC collected in Guangzhou and found that its mass absorption efficiency (MAE) at 365 nm was 0.52 m^2 g^{-1} in autumn and 0.92 m^2 g^{-1} in winter. Kuang et al. (2015) conducted an analysis based on positive matrix factorization and found that the relative contributions of BB, the secondary sulfate formation process, and ship emissions and sea salt in Guangzhou to humic-like substances carbon (HULIS-C), i.e., the hydrophobic part of WSOC, were 11–28%, 62–82%, and 7–19%, respectively. Despite this, both the emission sources and optical properties of ws-BrC in Guangzhou remain poorly constrained overall, with only a few studies using the powerful and feasible analytical tools (e.g., isotopes) to characterize ws-BrC surrogates (e.g., WSOC and HULIS-C) in this populous city.

In this study, both WSOC and HULIS-C in Guangzhou were chemically isolated from filter-based samples with the objectives of: 1) simultaneously measuring the mass concentrations and optical properties of these two ws-BrC surrogates; 2) studying the relative contributions of key emission sources using the cutting-edge tool of source apportionment, and 3) exploring the potential relationship between emission sources and the light absorption of ws-BrC in Guangzhou. The source apportionment of WSOC and HULIS-C were constrained by the analysis of radiocarbon (^{14}C, half-life = 5730 years), which is an excellent tracer for distinguishing fossil (e.g., coal, petroleum, and natural gas) from non-fossil sources (e.g., wood, grass, and biogenic emissions). This is because all ^{14}C atoms have completely decayed in fossil fuels, whereas the ^{14}C signal is constant in living organisms. Currently, ^{14}C is mainly used in the source identification of OC and EC (Lewis et al., 2004; Szidat et al., 2007; Zencak et al., 2007; Gustafsson et al., 2009; Szidat, 2009; Zotter et al., 2014; Zhang et al., 2015; Liu et al., 2016a; Winiger et al., 2016; Liu et al., 2017; Mouteva et al., 2017), and few studies have explored the ^{14}C signals of WSOC (Szidat et al., 2004; Kirillova et al., 2014a; Liu et al., 2014) and HULIS-C (Song et al., 2012). Additionally, the stable carbon isotope (^{13}C) was measured to constrain the emission sources and potential atmospheric processes of WSOC and HULIS-C in this study. To the best of our knowledge, this is the first study to quantify the effects of fossil and non-fossil sources on light absorption by ws-BrC, and the findings provide new insights into the origins of atmospheric ws-BrC and its implications in climate models.

2. Materials and methods

2.1. Sampling location and process

The sampling site was located on the roof of the library building of the Guangzhou Institute of Geochemistry (GIG), Chinese Academy of Sciences (CAS), Tianhe District, Guangzhou, China (Fig. 1). This location is surrounded by expressways, residential areas, and business zones, and is therefore considered to be an urban aerosol monitoring site. According to previous studies, the main sources of atmospheric aerosols in Guangzhou are traffic exhaust, coal combustion, BB, and cooking (Huang et al., 2014). In this study, we collected 12 samples of total suspended particles (TSP, 24 h) and one field blank (exposed to air for 5 min) on quartz fiber filters (QFF) during December 13–27, 2012, using a high-volume air sampler (TH-1000, Wuhan Tianhong Instrument Co., Ltd., Wuhan, China). All QFFs were pre-combusted at 450 °C for 6 h in a muffle furnace to remove any organic contaminants. After sampling, all filters were packed in aluminum foil and stored in a refrigerator at −20 °C prior to analysis.

2.2. Chemical analysis

2.2.1. OC and EC

Prior to determining OC and EC, an acidification procedure was performed to remove any carbonate in the TSP samples (Kirillova et al., 2014a). In brief, a piece of filter sample with a diameter of 5 cm was carefully cut out and placed in an open glass Petri dish. It was then acidified in a desiccator with 12 M hydrochloric acid for 24 h and dried at 60 °C for 1 h. OC and EC concentrations were determined using a commercial carbon analyzer (Sunset Laboratory Inc., Tigard, OR, USA), following the EUSSAR_2 temperature ramp (Cavalli et al., 2010). The uncertainties of the OC and EC measurements were 5.7% and 6.5%, respectively (Liu et al., 2017).

2.2.2. WSOC and HULIS-C

An area of the filter was extracted by ultra-sonication for 30 min using ultrapure water. The extract was then filtered slightly to remove particles, and the carbon in the filtrate was defined as the WSOC fraction. For HULIS-C isolation, a portion of the WSOC solution was adjusted to pH 2 and pipetted into a solid phase extraction cartridge (Oasis HLB, 30 μm, 60 mg, Waters, USA), and then HULIS-C was eluted into a vial with 2% (v/v) ammonia/methanol and dried completely under a stream

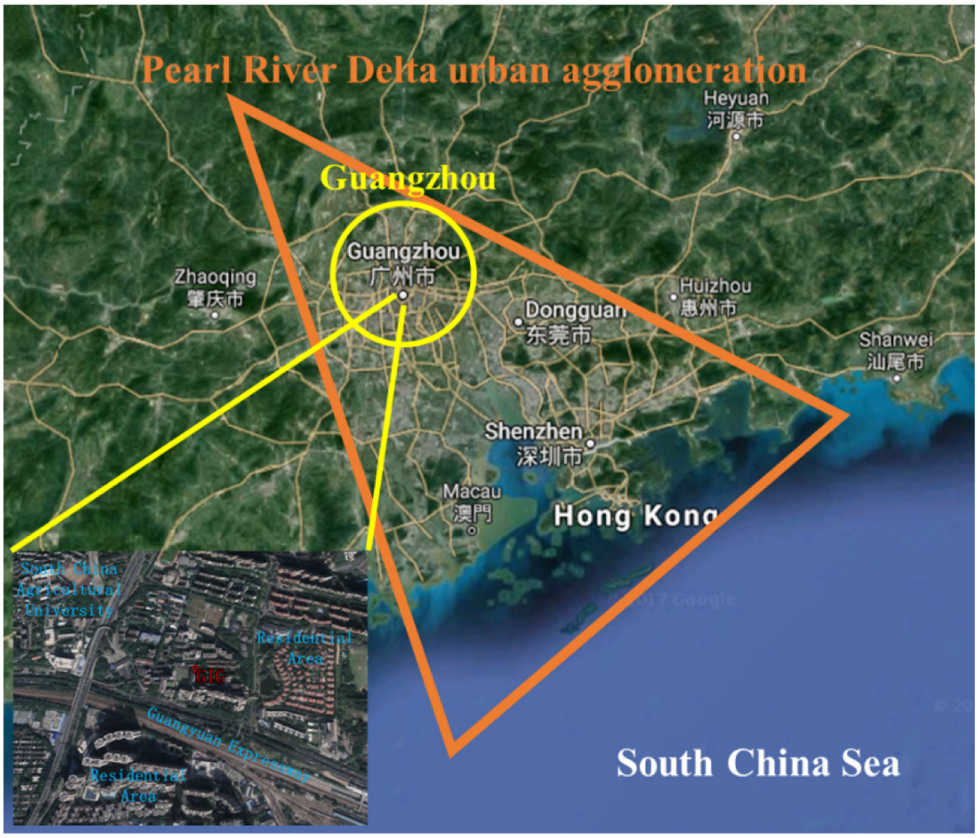

Fig. 1. The geographic position of Guangzhou and the sampling site (GIG).

of pure nitrogen to remove methanol. The HULIS-C was then re-dissolved using 30 mL ultrapure water. The detailed procedures of the HULIS isolation were reported previously (Lin et al., 2010; Mo et al., 2017). WSOC and HULIS-C were quantified by a laboratory total organic carbon (TOC) analyzer (Sievers M9, GE Analytical Instruments, Boulder, CO, USA). The carbon amounts in the WSOC and HULIS-C in the field blanks were 0.23 and 1.52 μg C/cm^2, respectively. All of the reported carbon fraction concentrations in this study were blank corrected.

2.2.3. Water-soluble inorganic ions

An area of the filter sample was punched out, extracted in ultra-pure water (10 mL), sonicated in an ice-water bath, and then filtered through a 0.22 μm size filter (Millipore, USA). The water extracts were finally injected into an ion chromatography column (Metrohm 883 Basic IC plus, Switzerland) for the determination of water-soluble inorganic ions (e.g., SO_4^{2-}, NO_3^-, NH_4^+, Cl^-, Na^+, Ca^{2+}, K^+, and Mg^{2+}).

2.3. Analysis of radiocarbon and stable carbon isotopes

The WSOC and HULIS-C solutions were frozen, freeze-dried, and combusted to CO_2 at 850 °C in a quartz tube with silver wire and CuO grains. The tube was then cracked, and the CO_2 released was further purified in a vacuum system and prepared for a graphite target using a method described previously (Xu et al., 2007) at the State Key Laboratory of Isotope Geochemistry, CAS (Ding et al., 2010; Ding et al., 2015; Liu et al., 2017). The ^{14}C signal of the graphite target was determined at the Institute of Heavy Ion Physics, Peking University using a compact AMS (National Electrostatics Corp., Middleton, WI, USA). All ^{14}C results were expressed as the fraction of modern carbon (f_m), with an average uncertainty of 0.43 ± 0.21%. The f_m values for the WSOC and HULIS field blanks were 0.6370 ± 0.0056 and 0.3291 ± 0.0037, respectively, which were used to correct the f_m values of samples using the isotopic mass balance equation. The f_m was further converted into the fraction of contemporary carbon (f_c) by normalization with a conversion factor of 1.06 (Liu et al., 2014) to compensate for the excess ^{14}C produced by atomic weapon testing in the 1950s and 1960s. Then, the relative contribution (%) of fossil sources in WSOC and HULIS-C could be directly calculated as follows:

$$f_f = (1 - f_c) \times 100 \quad (1)$$

$$f_{nf} = f_c \times 100 \quad (2)$$

where f_f and f_{nf} represent the relative contributions of fossil and non-fossil sources for a given carbon fraction (WSOC and HULISC-C). The ^{13}C signals were analyzed in the State Key Laboratory of Loess and Quaternary Geology, Xi'an, China, using a mass spectrometer (MAT-251, Finnigan, Waltham, MA, USA). The typical precision for ^{13}C measurements was ±0.2 (Ding et al., 2010) and the results were reported as $\delta^{13}C$ using the Pee Dee Belemnite (PDB) standard.

2.4. Measurement of optical properties

The optical attenuation (ATN) of the ws-BrC solution was measured using a UV–visible spectrophotometer (UV-4802, Unico, Shanghai,

Table 1
Mass concentrations of carbon fractions (μg C/m^3) and the ratios of WSOC-to-OC and HULIS-C-to-WSOC in Guangzhou in winter.

	Minimum	Maximum	Average	St. Dev
OC	4.17	43.4	18.2	10.6
EC	1.92	23.6	9.00	6.54
WSOC	1.50	6.45	4.55	1.66
HULIS-C	0.76	3.71	2.29	0.89
WSOC-to-OC	0.15	0.39	0.29	0.07
HULIS-C-to-WSOC	0.43	0.59	0.50	0.05

Table 2
Pearson correlation coefficients for chemicals measured in this study.

	OC	EC	WSOC	HULIS-C	Cl^-	NO_3^-	SO_4^{2-}	Na^+	NH_4^+	K^+	Mg^{2+}	Ca^{2+}
OC	1											
EC	0.643	1										
WSOC	0.826**	0.674	1									
HULIS-C	0.747**	0.457	0.954**	1								
Cl^-	0.745**	0.793**	0.527	0.334	1							
NO_3^-	0.791**	0.522	0.826**	0.814**	0.493	1						
SO_4^{2-}	0.608	0.240	0.746**	0.760**	0.157	0.677	1					
Na^+	0.485	0.620	0.406	0.237	0.812**	0.452	−0.018	1				
NH_4^+	0.528	0.154	0.709**	0.765**	0.091	0.670	0.964**	−0.092	1			
K^+	0.856**	0.605	0.961**	0.935**	0.530	0.854**	0.820**	0.375	0.768**	1		
Mg^{2+}	0.133	−0.107	0.179	0.226	0.141	0.430	0.070	0.589	0.097	0.168	1	
Ca^{2+}	0.863**	0.873**	0.742**	0.571	0.834**	0.731**	0.425	0.673	0.295	0.756**	0.102	1

** $p < 0.01$.

China) with a monitoring wavelength (λ) ranging from 200 to 800 nm (Mo et al., 2017). In addition to on-line measurements, this solution-based method can simply and effectively determine the light absorption of atmospheric ws-BrC, and has been widely applied in the atmospheric sciences (Hecobian et al., 2010; Cheng et al., 2011; Kirillova et al., 2014a; Cheng et al., 2017; Yan et al., 2017). The absorption coefficient of ws-BrC in the WSOC and HULIS-C was calculated as follows:

$$Abs_\lambda = (ATN_\lambda - ATN_{700}) \times [V_{solution} \div (V_{air} \times L)] \times \ln(10) \quad (3)$$

where Abs_λ is the absorption coefficient (Mm^{-1}) for a given wavelength, $V_{solution}$ (mL) is the volume of water used for extraction, and V_{air} (m^3) is the volume of sampled air, and L is the optical path length (0.01 m). The mass MAE_λ ($m^2\ g^{-1}$ C) and the wavelength dependence were then calculated as follows:

$$MAE_\lambda = Abs_\lambda \div C_i \quad (4)$$

$$Abs_\lambda = K \times \lambda^{-AAE} \quad (5)$$

where C_i is the atmospheric concentration (μg C/m^3) of WSOC or HULIS-C, AAE is the absorption Ångstrom exponent, and K is a fitting parameter. AAE was calculated by a linear regression of $\log_{10}(Abs_\lambda)$ on $\log_{10}(\lambda)$ from 310 to 450 nm(Cheng et al., 2016).

3. Results and discussion

3.1. Characteristics of WSOC and HULIS-C in Guangzhou in winter

Table 1 lists the mass concentrations of measured WSOC and HULIS-C. The average WSOC mass concentration was 4.55 ± 1.66 μg C/m^3 during the sampling campaign, accounting for 29 ± 7% of all OC. The TSP-based WSOC concentration was only 15% higher than the $PM_{2.5}$-based WSOC during the same period (Liu et al., 2014), suggesting that most WSOC particles are <2.5 μm in diameter. The average HULIS-C concentration was 2.29 ± 0.89 μg C/m^3, with a range from 0.76 to 3.71 μg C/m^3. The percentage of HULIS-C in WSOC was 50 ± 5%. These results are comparable to previous studies conducted in Guangzhou. For example, Fan et al. (2016a) found that the average HULIS-C concentration was 3.6 ± 2.0 μg C/m^3 in Guangzhou from October 2010 to January 2011, accounting for 56% of all WSOC. Table 2 lists the correlation coefficients for the relations among WSOC, HULIS-C, and other chemicals measured in this study. HULIS-C was significant correlated with WSOC ($r = 0.954$, $p < 0.01$), indicating a common emission source and/or formation process in the atmosphere. Additionally, both WSOC and HULIS-C were significantly ($p < 0.01$) correlated with all secondary water-soluble ions (e.g., NH_4^+, NO_3^-, and SO_4^{2-}) and the BB tracer (K^+), suggesting that secondary formation and BB are important sources of these two carbon fractions. In contrast, primary emissions from fossil-fuel-related activities, such as vehicles probably played a less important role in controlling the WSOC and HULIS-C concentration than non-fossil sources in this study, because neither displayed a significant correlation ($p < 0.01$) with EC (Table 2), which is a good tracer of primary emissions and mainly originates from fossil fuel combustion in urban areas (Pöschl, 2005).

The light absorption of solvent extracts at 365 nm is generally characterized as the optical properties of ws-BrC aerosols. In this study, the Abs_{365} value was 3.03 ± 1.37 Mm^{-1} (range: 1.22–6.07 Mm^{-1}) and 3.57 ± 1.34 Mm^{-1} (range: 1.45–6.28 Mm^{-1}) for HULIS-C and WSOC, respectively (Table 3). On average, $Abs_{365\text{-HULIS-C}}$ accounted for 83 ± 10% of $Abs_{365\text{-WSOC}}$, suggesting that HULIS-C dominates the light absorption of WSOC at 365 nm. The $MAE_{365\text{-HULIS-C}}$ was 1.33 ± 0.21 $m^2\ g^{-1}$ C (1.03–1.64 $m^2\ g^{-1}$ C), which is 66 ± 17% (30–94%) higher than that of $MAE_{365\text{-WSOC}}$ (0.81 ± 0.16 $m^2\ g^{-1}$ C on average, ranging from 0.55 to 1.04 $m^2\ g^{-1}$ C). The average AAE values for WSOC and HULIS were 5.33 ± 0.71 and 4.39 ± 0.53, respectively, indicating that HULIS-C is less spectrum dependent than WSOC.

We compared the optical properties of ws-BrC determined in this study with those reported previously (Fig. 2). The levels of AAE and MAE_{365} in Guangzhou were consistent with values reported in other regions, and we further found that ws-BrC was generally more absorptive in winter than in summer. For example, the $MAE_{365\text{-WSOC}}$ value in winter (>1 $m^2\ g^{-1}$ C) was more than twice as high as that in summer (~0.5 $m^2\ g^{-1}$ C) in Beijing, China (Fig. 2). This phenomenon has also been observed in developed countries such as Korea and the USA, where the air is less polluted. Because BB is thought to be an important emitter of ws-BrC at the regional and global scales (Chen and Bond, 2010; Arola et al., 2011), it is reasonable to assume that the general trend of a higher $MAE_{365\text{-WSOC}}$ in winter is caused by BB, such as wood fuel, agricultural residue, and grass. The results of chamber studies

Table 3
Optical properties of WSOC and HULIS-C.

	Abs_{365}			MAE_{365}			AAE		
	Range	Average	StDev	Range	Average	StDev	Range	Average	StDev
WSOC	1.45–6.28	3.57	1.34	0.55–1.04	0.81	0.16	4.03–6.16	5.33	0.71
HULIS-C	1.22–6.07	3.03	1.37	1.03–1.64	1.33	0.21	3.12–5.17	4.39	0.53
HULIS-C/WSOC	0.68–0.97	0.83	0.10	1.30–1.94	1.66	0.17	0.73–1.08	0.83	0.10

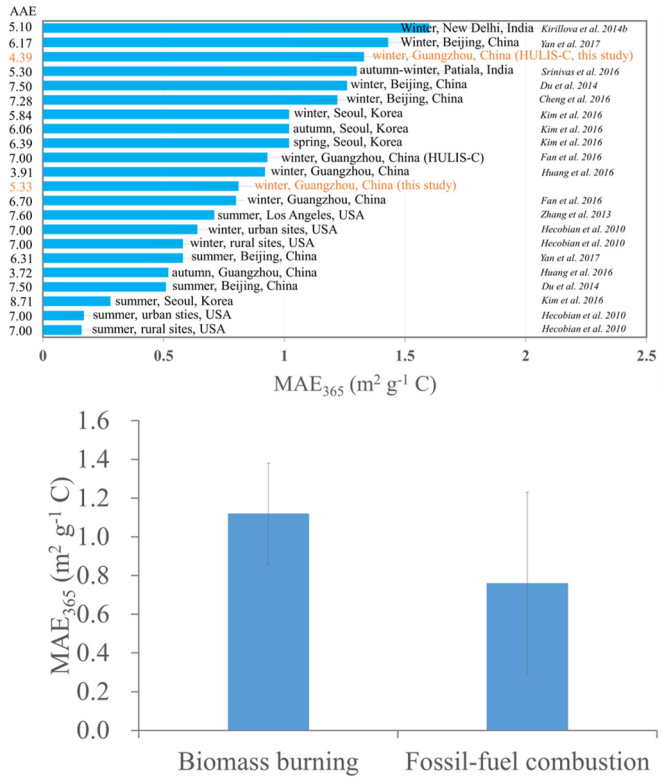

Fig. 2. A comparison of optical properties for water-soluble BrC around the world (top panel) and the results from emission sources (down panel). Data were obtained from the references of (Hecobian et al., 2010; Zhang et al., 2013; Du et al., 2014; Kirillova et al., 2014b; Cheng et al., 2016; Fan et al., 2016b; Huang et al., 2016; Kim et al., 2016; Park and Yu, 2016; Srinivas et al., 2016; Yan et al., 2017).

partly support this finding (Fig. 2), with the average $MAE_{365\text{-}WSOC}$ of BB (1.12 ± 0.26 m^2 g^{-1} C) being ~ 45% higher than that of fossil fuel combustion (0.76 ± 0.47 m^2 g^{-1} C).

3.2. Source apportionment based on ^{14}C measurements and the ^{13}C fingerprint

Measurements of ^{14}C showed that most WSOC and HULIS-C in this study were associated with non-fossil sources, but the influence of fossil fuels could not be neglected (Table 4). The relative contributions of fossil and non-fossil sources to WSOC were $33.7 \pm 5.0\%$ (22.3–41.9%) and $66.3 \pm 5.0\%$ (58.1–77.7%), respectively. This result corresponds to our previous findings that 34% (27–38%) of $PM_{2.5}$-based WSOC in Guangzhou was derived from fossil sources during the same season (Liu et al., 2014). In remote sites (e.g., Jianfengling in Hainan Island and Hanimaadhoo in the Maldives) and less polluted cities (e.g., Bern, Zürich, Göteborg and Sapporo), the contribution of fossil sources was generally only ~15% (data was obtained from the references of Liu et al., 2016b), which in turn suggests anthropogenic activities have an important effect on WSOC levels in Guangzhou. Much higher contributions (~50%) of fossil sources to WSOC has been reported in north China (Kirillova et al., 2014a; Yan et al., 2017), which is probably due to the extensive use of coal in that region.

Table 4
Radiocarbon-based relative contributions (%) of fossil and non-fossil sources in WSOC and HULIS-C.

Sampling day	WSOC		HULIS-C	
	Non-fossil	Fossil	Non-fossil	Fossil
Dec.13	60.6 ± 4.8	39.4 ± 4.8	55.8 ± 4.2	44.2 ± 4.2
Dec.16	58.1 ± 5.1	41.9 ± 5.1	53.7 ± 4.1	46.3 ± 4.1
Dec.17	68.6 ± 6.0	31.4 ± 6.0	69.3 ± 5.3	30.7 ± 5.3
Dec.18	64.5 ± 8.8	35.5 ± 8.8	75.7 ± 9.1	24.3 ± 9.1
Dec.19	64.5 ± 6.6	35.5 ± 8.8	64.3 ± 5.1	35.7 ± 5.1
Dec.20	65.3 ± 4.9	34.7 ± 4.9	61.2 ± 4.5	38.8 ± 4.5
Dec.21	68.7 ± 6.4	31.3 ± 6.4	65.6 ± 5.2	34.4 ± 5.2
Dec.22	71.3 ± 7.1	28.7 ± 7.1	71.0 ± 5.7	29.0 ± 5.7
Dec.23	64.3 ± 5.6	35.7 ± 5.6	59.6 ± 4.6	40.4 ± 4.6
Dec.24	62.9 ± 4.9	37.1 ± 4.9	54.1 ± 3.9	45.9 ± 3.9
Dec.25	69.7 ± 5.3	30.3 ± 5.3	64.3 ± 4.7	35.7 ± 4.7
Dec.26	77.8 ± 5.6	22.2 ± 5.6	76.1 ± 5.4	23.9 ± 5.4
Average	66.3 ± 5.0	33.7 ± 5.0	64.2 ± 7.4	35.8 ± 7.4

Table 5
$\delta^{13}C$ values of WSOC and HULIS-C in this study.

Sampling day	WSOC	HULIS-C
Dec.13	−24.3	−25.9
Dec.16	−24.5	−25.2
Dec.17	−24.6	−23.4
Dec.18	−22.5	–
Dec.19	−22.4	−24.6
Dec.20	−22.5	−24.8
Dec.21	−25.5	–
Dec.22	−25.7	−24.5
Dec.23	−23.8	−23.4
Dec.24	−23.1	−23.0
Dec.25	−23.2	−23.2
Dec.26	−22.2	−23.9
Average	−23.7 ± 1.2	−24.2 ± 0.9

–: sample failed to measure.

No significant difference was observed in the ^{14}C signals between HULIS-C and WSOC (Table 4). The contributions of fossil and non-fossil sources to HULIS-C were $35.8 \pm 7.4\%$ (23.9–46.3%) and $64.2 \pm 7.4\%$ (53.7–76.1%), respectively. In principle, OC directly emitted from fossil fuel combustion is water-insoluble (Weber et al., 2007; Dai et al., 2015), and the fossil fractions in WSOC and HULIS-C are therefore mainly derived from the oxidation of precursor gases and/or the aging process. Overall, these ^{14}C results show that two-thirds of the ws-BrC proxies in Guangzhou were derived from non-fossil sources and the remaining one-third originated from fossil sources.

The $\delta^{13}C$ values of WSOC and HULIS-C were -23.7 ± 1.2‰ (−25.7 to −22.2‰) and -24.2 ± 0.9‰ (−25.9 to −23.0‰), respectively (Table 5). These $\delta^{13}C$ values are within the range of major sources (−40 to −10‰) and close to the fingerprint values of coal, petroleum, and C3 plants (Fig. 3), which suggests that other sources, such as C4 plants (e.g., corn and sugarcane) and natural gas, play a limited role in the formation of WSOC and HULIS-C in Guangzhou. Because air masses reaching Guangzhou in winter are predominately derived from the northern part of the continent, the effect of marine aerosols on the ^{13}C signal is limited and can be ignored. This result confirms a previous study that $\delta^{13}C$ measurement is useful for distinguishing among the major sources of the carbon fractions in China (Cao et al., 2011). Additionally, $\delta^{13}C$ values can be affected by atmospheric processing due to

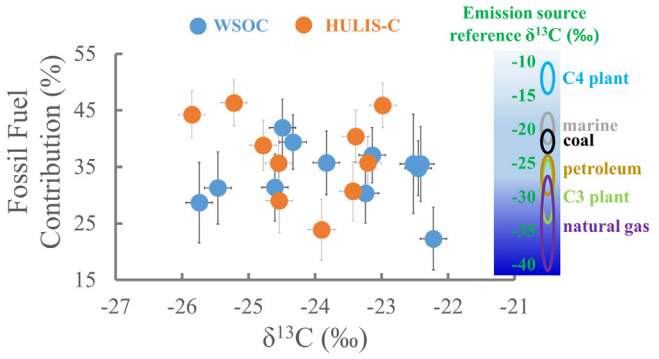

Fig. 3. ^{14}C-based fossil fuel contribution (%) in WSOC and HULIS-C versus $\delta^{13}C$ signals. The $\delta^{13}C$ values of emission sources were obtained from (Kirillova et al., 2014a and the references therein).

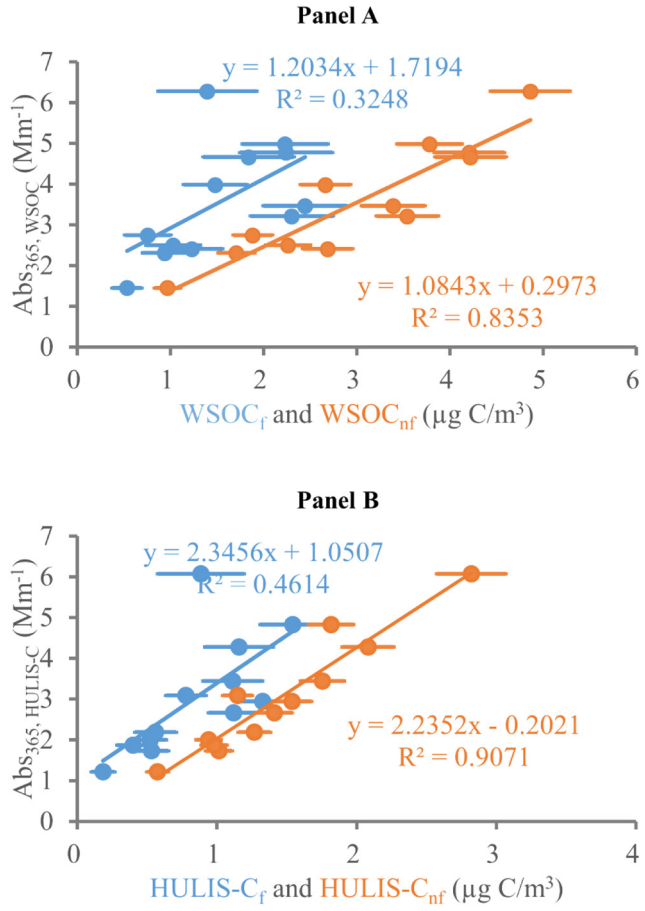

Fig. 4. Correlations between Abs_{365} and the concentrations of fossil and non-fossil carbons. Panel A: WSOC; Panel B: HULIS-C.

the kinetic isotope effect. Kirillova et al. (2013) found that the $\delta^{13}C$-WSOC value lineally increased with an increase in ^{14}C levels during the aging of WSOC collected at two remote South Asian sites (Hanimaadhoo Island in the Indian Ocean and a hilltop site at Sinhagad in the west of India), although this phenomenon was not observed in this study (Fig. 3). One possible explanation for this is that the aging process probably had much less influence on our samples than those collected in remote sites in South Asia.

3.3. Contributions of fossil and non-fossil carbon to light-absorption at 365 nm

Little is known about the relative contribution of different sources in ws-BrC light absorption. As shown in Fig. 4, levels of non-fossil WSOC

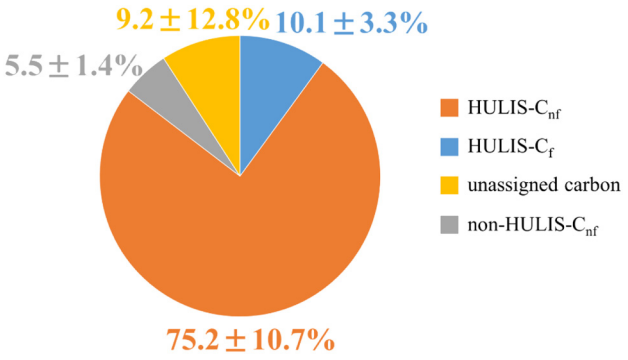

Fig. 5. Source apportionment of light-absorption at 365 nm for ws-BrC in Guangzhou.

($WSOC_{nf}$) were correlated well with $Abs_{365\text{-}WSOC}$ ($R^2 = 0.84$), whereas a much weaker correlation ($R^2 = 0.32$) was observed for fossil WSOC ($WSOC_f$). Better correlation coefficients were found for the relation between HULIS-C light absorption and the HULISC-C concentration (Fig. 4). The R^2 values for non-fossil carbon ($WSOC_{nf}$ and HULIS-C_{nf}) were approximately double the values for fossil carbon ($WSOC_f$ and HULIS-C_f), indicating that non-fossil sources played a more important role than fossil sources in light-absorption by ws-BrC.

To quantify the relative contributions of the different carbon fractions to light absorption by ws-BrC, we performed a multiple linear regression (CI = 95%) for the relationship of the sub-fractions of WSOC, i.e., HULIS-C_f, HULIS-C_{nf}, non-HULIS-C_f, and non-HULIS-C_{nf}, with $Abs_{365\text{-}WSOC}$. Because the correlation between non-HULIS-C_f and $Abs_{365\text{-}WSOC}$ was very weak ($R^2 < 0.1$), this carbon fraction was not likely to light absorption at 365 nm and was not considered in the fitting regression. The corresponding R^2 values were 0.48, 0.87, and 0.64 for HULIS-C_f, HULIS-C_{nf}, and non-HULIS-C_{nf}, respectively. The fitting output resulted in multiple R, R^2, and F-values of 0.94, 0.88, and 0.0004, respectively. The relative uncertainty was in the range of −22% to +34%. The regression equations were as follows:

$$Abs_{365-WSOC}\left(Mm^{-1}\right) = Abs_{365-WSOC}(HULIS-C_f) + Abs_{365-WSOC}(HULIS-C_{nf}) + Abs_{365-WSOC}(non-HULIS-C_{nf}) + K \quad (6)$$

$$Abs_{365-WSOC}(HULIS-C_f) = 0.431 \pm 0.781\,(m^2\ g^{-1}C) \times HULIS-C_f\,(\mu g\ C/m^3) \quad (7)$$

$$Abs_{365-WSOC}(HULIS-C_{nf}) = 1.850 \pm 0.449\,(m^2\ g^{-1}C) \times HULIS\text{-}C_{nf}\,(\mu g\ C/m^3) \quad (8)$$

$$Abs_{365-WSOC}(non\text{-}HULIS-C_{nf}) = 0.124 \pm 0.628\,(m^2\ g^{-1}\ C) \times non\text{-}HULIS-C_{nf}\,(\mu g\ C/m^3) \quad (9)$$

$$K = 0.335 \pm 0.460\ \left(Mm^{-1}\right) \quad (10)$$

where $Abs_{365\text{-}WSOC}$ (HULIS-C_f), $Abs_{365\text{-}WSOC}$ (HULIS-C_{nf}), and $Abs_{365\text{-}WSOC}$ (non-HULIS-C_{nf}) are the light-absorptions (Mm^{-1}) of fossil HULIS-C, non-fossil HULIS-C, and non-fossil non-HULIS-C, respectively. K is a constant (Mm^{-1}). According to these equations, the MAE_{365} values for HULIS-C_f, HULIS-C_{nf}, and non-HULIS-C_{nf} are 0.431 ± 0.781, 1.850 ± 0.449, and 0.124 ± 0.628 $m^2\ g^{-1}$ C, respectively. These modeled MAE_{365} values for HULIS-C_f and HULIS-C_{nf} correspond to those from coal combustion (0.63 $m^2\ g^{-1}$ C) and BB (0.97–2.09 $m^2\ g^{-1}$ C) measured in chambers experiments (Fan et al., 2016b), implying that these carbon fractions are likely directly emitted by fuel burning. The MAE_{365} of non-HULIS-C_{nf} was much lower than that of the former two carbon fractions. Given that lower MAE_{365} values generally occurred during summer (Fig. 2) when secondary organic aerosols (SOAs) were more easily formed and there was little absorbance by biogenic SOA (Xie et al., 2017), the non-HULIS-C_{nf} fraction with a low MAE_{365} was probably mainly derived from the oxidation of biogenic volatile organic compounds. Light absorption at 365 nm occurred in the order HULIS-C_{nf} > HULIS-C_f > non-HULIS-C_{nf}.

On average, the contributions of HULIS-C_f, HULIS-C_{nf}, and non-HULIS-C_{nf} to the total light absorption by ws-BrC were 10.1 ± 3.3%, 75.2 ± 10.7%, and 5.5 ± 1.4%, respectively, with the remaining contributions derived from unassigned matter (Fig. 5). Therefore, the total contributions to overall light absorption by ws-BrC from fossil and non-fossil carbon (HULIS-C_{nf} plus non-HULIS-C_{nf}) in Guangzhou in winter were approximately ~10 and ~80%, respectively. As mentioned above, the HULIS-C_{nf} fraction was likely to be predominately derived from BB, because the burning of agricultural residues and wood fuels are the main sources of ws-BrC responsible for light absorption. Considering that BB activities (e.g., field burning of crop residues) are generally

more severe in winter in South China (He et al., 2011; Ding et al., 2012; Wang et al., 2016), the annual contribution of BB to light absorption by ws-BrC should be lower than 80%, which in turn suggests that the corresponding contribution of fossil fuels would be higher than 10%. Overall, our understanding of the roles of ws-BrC is still poor and further isotopic studies are needed to further investigate its sources, especially in regions with high organic aerosol emissions, to offset the disparity between observations and models in radiative forcing by aerosols.

4. Conclusion

This study investigated the sources of mass and light absorption of two water-soluble ws-BrC surrogates, WSOC and HULIS-C, in the urban area of Guangzhou, China, through the measurement of dual carbon isotopes (^{14}C and ^{13}C). The mass concentration, MAE at 365 nm, and the AAE values at 310 to 450 nm were 4.55 ± 1.66 μg C/m^3, 0.81 ± 0.16 m^3 g^{-1} C, and 5.33 ± 0.71, respectively, for WSOC, and 2.29 ± 0.89 μg C/m^3, 1.33 ± 0.21 m^3 g^{-1} C, and 4.39 ± 0.53, respectively, for HULIS-C. The ^{14}C results revealed that two-thirds and one-thirds of ws-BrC surrogates were derived from biomass and fossil fuels, respectively. The analysis of ^{13}C further constrained the sources of WSOC and HULIS-C to C3 plants, coal, and petroleum. The contribution of fossil fuel to light absorption by ws-BrC was found to be small but cannot be ignored (~10%). The largest contributor to light absorption by ws-BrC was non-fossil HULIS-C (~75%) fraction, which was predominantly derived from BB. These data can be used to improve the modelling of the climate forcing of aerosols.

Acknowledgments

We gratefully acknowledge the project funding from the Natural Science Foundation of China (grant numbers 41430645, 41773120, and 41603096), the Guangzhou Science and Technology Program Key Projects (No. 201504010002) and the State Key Laboratory of Organic Geochemistry (SKLOGA201603A).

References

Alexander, D.T.L., Crozier, P.A., Anderson, J.R., 2008. Brown carbon spheres in East Asian outflow and their optical properties. Science 321 (5890), 833–836.
Andreae, M.O., Gelencsér, A., 2006. Black carbon or brown carbon? The nature of light-absorbing carbonaceous aerosols. Atmos. Chem. Phys. 6 (10), 3131–3148.
Arola, A., Schuster, G., Myhre, G., Kazadzis, S., Dey, S., Tripathi, S.N., 2011. Inferring absorbing organic carbon content from AERONET data. Atmos. Chem. Phys. 11 (1), 215–225.
Bond, T.C., 2001. Spectral dependence of visible light absorption by carbonaceous particles emitted from coal combustion. Geophys. Res. Lett. 28 (21), 4075–4078.
Bond, T.C., Zarzycki, C., Flanner, M.G., Koch, D.M., 2011. Quantifying immediate radiative forcing by black carbon and organic matter with the specific forcing pulse. Atmos. Chem. Phys. 11, 1505–1525.
Cao, J., Lee, S.C., Ho, K.F., Zhang, X., Zou, S., Fung, K., Chow, J.C., Watson, J.G., 2003. Characteristics of carbonaceous aerosol in Pearl River Delta Region, China during 2001 winter period. Atmos. Environ. 37 (11), 1451–1460.
Cao, J.-j., Chow, J.C., Tao, J., Lee, S.-c., Watson, J.G., Ho, K.-f., Wang, G.-h., Zhu, C.-s., Han, Y.-m., 2011. Stable carbon isotopes in aerosols from Chinese cities: Influence of fossil fuels. Atmos. Environ. 45 (6), 1359–1363.
Cavalli, F., Viana, M., Yttri, K.E., Genberg, J., Putaud, J.-P., 2010. Toward a standardised thermal-optical protocol for measuring atmospheric organic and elemental carbon: the EUSAAR protocol. Atmospheric Measurement Techniques 3 (1), 79–89.
Chen, Y., Bond, T., 2010. Light absorption by organic carbon from wood combustion. Atmos. Chem. Phys. 10 (4), 1773–1787.
Cheng, Y., He, K.-B., Zheng, M., Duan, F.-K., Du, Y.Z.-Y., Ma, Y.-L., Tan, J.-H., Yang, F.-M., Liu, J.-M., Zhang, X.-L., 2011. Mass absorption efficiency of elemental carbon and water-soluble organic carbon in Beijing, China. Atmos. Chem. Phys. 11 (22), 11497–11510.
Cheng, Y., He, K.-b., Du, Z.-y., Engling, G., Liu, J.-m., Ma, Y.-l., Zheng, M., Weber, R.J., 2016. The characteristics of brown carbon aerosol during winter in Beijing. Atmos. Environ. 127, 355–364.
Cheng, Y., He, K.-b., Engling, G., Weber, R., Liu, J.-m., Du, Z.-y., Dong, S.-p., 2017. Brown and black carbon in Beijing aerosol: Implications for the effects of brown coating on light absorption by black carbon. Sci. Total Environ. 599, 1047–1055.
Dai, S., Bi, X., Chan, L., He, J., Wang, B., Wang, X., Peng, P., Sheng, G., Fu, J., 2015. Chemical and stable carbon isotopic composition of PM2.5 from on-road vehicle emissions in the PRD region an implications for vehicl emission control policy. Atmos. Chem. Phys. 15, 3097–3108.
Deng, X., Tie, X., Wu, D., Zhou, X., Bi, X., Tan, H., Li, F., Jiang, C., 2008. Long-term trend of visibility and its characterizations in the Pearl River Delta (PRD) region, China. Atmos. Environ. 42 (7), 1424–1435.
Ding, P., Shen, C., Wang, N., Yi, W., Ding, X., Fu, D., Liu, K., Zhou, L., 2010. Turnover rate of soil organic matter and origin of soil 14 CO 2 in deep soil from a subtropical forest in Dinghushan Biosphere Reserve, South China. Radiocarbon 52 (3), 1422–1434.
Ding, X., Wang, X., Gao, B., Fu, X., He, Q., Zhao, X., Yu, J., Zheng, M., 2012. Tracer-based estimation of secondary organic carbon in the Pearl River Delta, south China. J. Geophys. Res.-Atmos. 117, D05313.
Ding, P., Shen, C., Yi, W., Wang, N., Ding, X., Liu, K., Fu, D., Liu, W., Liu, Y., 2015. A high resolution method for 14 C analysis of a coral from South China Sea: Implication for "AD 775" 14 C event. Nucl. Instrum. Methods Phys. Res., Sect. B 361, 659–664.
Du, Z., He, K., Cheng, Y., Duan, F., Ma, Y., Liu, J., Zhang, X., Zheng, M., Weber, R., 2014. A yearlong study of water-soluble organic carbon in Beijing II: Light absorption properties. Atmos. Environ. 89, 235–241.
Fan, X., Song, J., Peng, P.a., 2016a. Temporal variations of the abundance and optical properties of water soluble humic-like substances (HULIS) in PM 2.5 at Guangzhou, China. Atmos. Res. 172, 8–15.
Fan, X., Wei, S., Zhu, M., Song, J., Peng, P.a., 2016b. Comprehensive characterization of humic-like substances in smoke PM 2.5 emitted from the combustion of biomass materials and fossil fuels. Atmos. Chem. Phys. 16 (20), 13321–13340.
Feng, Y., Ramanathan, V., Kotamarthi, V., 2013. Brown carbon: a significant atmospheric absorber of solar radiation? Atmos. Chem. Phys. 13 (17), 8607–8621.
Gustafsson, Ö., Kruså, M., Zencak, Z., Sheesley, R.J., Granat, L., Engström, E., Praveen, P.S., Rao, P.S.P., Leck, C., Rodhe, H., 2009. Brown clouds over South Asia: biomass or fossil fuel combustion? Science 323 (5913), 495–498.
He, M., Zheng, J., Yin, S., Zhang, Y., 2011. Trends, temporal and spatial characteristics, and uncertainties in biomass burning emissions in the Pearl River Delta, China. Atmos. Environ. 45 (24), 4051–4059.
Hecobian, A., Zhang, X., Zheng, M., Frank, N., Edgerton, E.S., Weber, R.J., 2010. Water-Soluble Organic Aerosol material and the light-absorption characteristics of aqueous extracts measured over the Southeastern United States. Atmos. Chem. Phys. 10 (13), 5965–5977.
Huang, R., Zhang, Y., Bozzetti, C., Ho, K., Cao, J., Han, Y., Daellenbach, K., Slowik, J., Platt, S., Canonaco, F., Zotter, P., Wolf, R., Pieber, S., Bruns, E., Crippa, M., Ciarelli, G., Piazzalunga, A., Schwikowski, M., Abbaszade, G., Schnelle-Kreis, J., Zimmermann, R., An, Z., Szidat, S., Baltensperger, U., Haddad, E., Prevot, A., 2014. High secondary aerosol contribution to particulate pollution during haze events in China. Nature 514, 218–222.
Huang, H., Bi, X.-h., Peng, L., Wang, X.-m., Sheng, G.-y., Fu, J.-m., 2016. Light Absorption Properties of Water-Soluble Organic Carbon (WSOC) Associated with Particles in Autumn and Winter in the Urban Area of Guangzhou. Environmental Science (in Chinese) 1, 005.
Kanakidou, M., Seinfeld, J.H., Pandis, S.N., Barnes, I., Dentener, F., Facchini, M., Dingenen, R.V., Ervens, B., Nenes, A., Nielsen, C., Swietlicki, E., Putaud, J., Balkanski, Y., Fuzzi, S., Horth, J., Moortgat, G., Winterhalter, R., Myhre, C., Tsigaridis, K., Vignati, E., Stephanou, E., Wilson, J., 2005. Organic aerosol and global climate modelling: a review. Atmos. Chem. Phys. 5 (4), 1053–1123.
Kim, H., Kim, J.Y., Jin, H.C., Lee, J.Y., Lee, S.P., 2016. Seasonal variations in the light-absorbing properties of water-soluble and insoluble organic aerosols in Seoul, Korea. Atmos. Environ. 129, 234–242.
Kirillova, E.N., Andersson, A., Sheesley, R.J., Kruså, M., Praveen, P.S., Budhavant, K., Safai, P.D., Rao, P.S.P., Gustafsson, Ö., 2013. 13C-and 14C-based study of sources and atmospheric processing of water-soluble organic carbon (WSOC) in South Asian aerosols. J. Geophys. Res.-Atmos. 118 (2), 614–626.
Kirillova, E.N., Andersson, A., Han, J., Lee, M., Gustafsson, Ö., 2014a. Sources and light absorption of water-soluble organic carbon aerosols in the outflow from northern China. Atmos. Chem. Phys. 14 (3), 1413–1422.
Kirillova, E.N., Andersson, A., Tiwari, S., Srivastava, A.K., Bisht, D.S., Gustafsson, Ö., 2014b. Water-soluble organic carbon aerosols during a full New Delhi winter: Isotope-based source apportionment and optical properties. J. Geophys. Res.-Atmos. 119, 3476–3485.
Kirillova, E.N., Marinoni, A., Bonasoni, P., Vuillermoz, E., Facchini, M.C., Fuzzi, S., Decesari, S., 2016. Light absorption properties of brown carbon in the high Himalayas. J. Geophys. Res.-Atmos. 121 (16), 9621–9639.
Kuang, B., Lin, P., Huang, X.H.H., Yu, J., 2015. Sources of humic-like substances in the Pearl River Delta, China: positive matrix factorization analysis of PM 2.5 major components and source markers. Atmos. Chem. Phys. 15 (4), 1995–2008.
Kulmala, M., Asmi, A., Lappalainen, H.K., Baltensperger, U., Brenguier, J.L., Facchini, M.C., Hansson, H.C., Hov, O., O'Dowd, C.D., Poschl, U., Wiedensohler, A., Boers, R., Boucher, O., de Leeuw, G., van der Gon, H., Feichter, J., Krejci, R., Laj, P., Lihavainen, H., Lohmann, U., McFiggans, G., Mentel, T., Pilinis, C., Riipinen, I., Schulz, M., Stohl, A., Swietlicki, E., Vignati, E., Alves, C., Amann, M., Ammann, M., Arabas, S., Artaxo, P., Baars, H., Beddows, D.C.S., Bergstrom, R., Beukes, J.P., Bilde, M., Burkhart, J.F., Canonaco, F., Clegg, S.L., Coe, H., Crumeyrolle, S., D'Anna, B., Decesari, S., Gilardoni, S., Fischer, M., Fjaeraa, A.M., Fountoukis, C., George, C., Gomes, L., Halloran, P., Hamburger, T., Harrison, R.M., Herrmann, H., Hoffmann, T., Hoose, C., Hu, M., Hyvarinen, A., Horrak, U., Iinuma, Y., Iversen, T., Josipovic, M., Kanakidou, M., Kiendler-Scharr, A., Kirkevag, A., Kiss, G., Klimont, Z., Kolmonen, P., Komppula, M., Kristjansson, J.E., Laakso, L., Laaksonen, A., Labonnote, L., Lanz, V.A., Lehtinen, K.E.J., Rizzo, L.V., Makkonen, R., Manninen, H.E., McMeeking, G., Merikanto, J., Minikin, A., Mirme, S., Morgan, W.T., Nemitz, E., O'Donnell, D., Panwar, T.S., Pawlowska, H., Petzold, A., Pienaar, J.J., Pio, C., Plass-Duelmer, C., Prevot, A.S.H., Pryor, S., Reddington, C.L., Roberts, G., Rosenfeld, D., Schwarz, J., Seland, O., Sellegri, K., Shen, X.J., Shiraiwa, M., Siebert, H., Sierau, B., Simpson, D., Sun, J.Y., Topping, D., Tunved, P., Vaattovaara, P., Vakkari, V., Veefkind, J.P., Visschedijk, A., Vuollekoski, H., Vuolo,

R., Wehner, B., Wildt, J., Woodward, S., Worsnop, D.R., van Zadelhoff, G.J., Zardini, A.A., Zhang, K., van Zyl, P.G., Kerminen, V.M., Carslaw, K.S., Pandis, S.N., 2011. General overview: European Integrated project on Aerosol Cloud Climate and Air Quality interactions (EUCAARI) - integrating aerosol research from nano to global scales. Atmos. Chem. Phys. 11 (24), 13061–13143.

Lai, S., Zhao, Y., Ding, A., Zhang, Y., Song, T., Zheng, J., Ho, K.F., Lee, S.-c., Zhong, L., 2016. Characterization of pm 2.5 and the major chemical components during a 1-year campaign in rural Guangzhou, southern China. Atmos. Res. 167, 208–215.

Lan, Z., Zhang, B., Huang, X., Zhu, Q., Yuan, J., Zeng, L., Hu, M., He, L., 2017. Source apportionment of PM2. 5 light extinction in an urban atmosphere in China. Sciences, Journal of Environmental.

Laskin, A., Laskin, J., Nizkorodov, S.A., 2015. Chemistry of Atmospheric Brown Carbon. Chem. Rev. 115 (10), 4335–4382.

Lewis, C.W., Klouda, G.A., Ellenson, W.D., 2004. Radiocarbon measurement of the biogenic contribution to summertime PM2.5 ambient aerosol in Nashville, TN. Atmos. Environ. 38 (35), 6053–6061.

Lin, P., Huang, X.-F., He, L.-Y., Yu, J.Z., 2010. Abundance and size distribution of HULIS in ambient aerosols at a rural site in South China. J. Aerosol Sci. 41 (1), 74–87.

Lin, G., Penner, J.E., Flanner, M.G., Sillman, S., Xu, L., Zhou, C., 2014a. Radiative forcing of organic aerosol in the atmosphere and on snow: Effects of SOA and brown carbon. J. Geophys. Res.-Atmos. 119 (12), 7453–7476.

Lin, Y.-H., Budisulistiorini, S.H., Chu, K., Siejack, R.A., Zhang, H., Riva, M., Zhang, Z., Gold, A., Kautzman, K.E., Surratt, J.D., 2014b. Light-absorbing oligomer formation in secondary organic aerosol from reactive uptake of isoprene epoxydiols. Environ. Sci. Technol. 48 (20), 12012–12021.

Lin, P., Bluvshtein, N., Rudich, Y., Nizkorodov, S.A., Laskin, J., Laskin, A., 2017. Molecular chemistry of atmospheric brown carbon inferred from a nationwide biomass burning event. Environ. Sci. Technol. 51 (20), 11561–11570.

Liu, J., Li, J., Zhang, Y., Liu, D., Ding, P., Shen, C., Shen, K., He, Q., Ding, X., Wang, X., Chen, D., Szidat, S., Zhang, G., 2014. Source Apportionment using radiocarbon and organic tracers for PM2.5 carbonaceous aerosols in guangzhou, South China: contrasting local-and regional-scale haze events. Environ. Sci. Technol. 48, 12002–12011.

Liu, J., Scheuer, E., Dibb, J., Diskin, G.S., Ziemba, L.D., Thornhill, K.L., Anderson, B.E., Wisthaler, A., Mikoviny, T., Devi, J.J., Bergin, M., Perring, A.E., Markovic, M.Z., Schwarz, J.P., Campuzano-Jost, P., Day, D.A., Jimenez, J.L., Weber, R.J., 2015. Brown carbon aerosol in the North American continental troposphere: sources, abundance, and radiative forcing. Atmos. Chem. Phys. 15, 7841–7858.

Liu, J., Li, J., Liu, D., Ding, P., Shen, C., Mo, Y., Wang, X., Luo, C., Cheng, Z., Szidat, S., Zhang, Y., Chen, Y., Zhang, G., 2016a. Source apportionment and dynamic changes of carbonaceous aerosols during the haze bloom-decay process in China based on radiocarbon and organic molecular tracers. Atmos. Chem. Phys. 16 (5), 2985–2996.

Liu, J., Li, J., Vonwiller, M., Liu, D., Cheng, H., Shen, K., Salazar, G., Agrios, K., Zhang, Y., He, Q., Ding, X., Zhong, G., Wang, X., Szidat, S., Zhang, G., 2016b. The importance of non-fossil sources in carbonaceous aerosols in a megacity of central China during the 2013 winter haze episode: A source apportionment constrained by radiocarbon and organic tracers. Atmos. Environ. 144, 60–68.

Liu, J., Li, J., Ding, P., Zhang, Y., Liu, D., Shen, C., Zhang, G., 2017. Optimizing isolation protocol of organic carbon and elemental carbon for 14 C analysis using fine particulate samples. Atmos. Environ. 154, 9–19.

Ma, X., Yu, F., Luo, G., 2012. Aerosol direct radiative forcing based on GEOS-Chem-APM and uncertainties. Atmos. Chem. Phys. 12, 5563–5581.

Mo, Y., Li, J., Liu, J., Zhong, G., Cheng, Z., Tian, C., Chen, Y., Zhang, G., 2017. The influence of solvent and pH on determination of the light absorption properties of water-soluble brown carbon. Atmos. Environ. 161, 90–98.

Mouteva, G.O., Randerson, J.T., Fahrni, S.M., Bush, S.E., Ehleringer, J.R., Xu, X., Santos, G.M., Kuprov, R., Schichtel, B.A., Czimczik, C.I., 2017. Using radiocarbon to constrain black and organic carbon aerosol sources in Salt Lake City. J. Geophys. Res.-Atmos. 122 (18), 9843–9857.

Olson, M.R., Victoria Garcia, M., Robinson, M.A., Van Rooy, P., Dietenberger, M.A., Bergin, M., Schauer, J.J., 2015. Investigation of black and brown carbon multiple-wavelength-dependent light absorption from biomass and fossil fuel combustion source emissions. J. Geophys. Res.-Atmos. 120 (13), 6682–6697.

Park, S.S., Yu, J., 2016. Chemical and light absorption properties of humic-like substances from biomass burning emissions under controlled combustion experiments. Atmos. Environ. 136, 114–122.

Pöschl, U., 2005. Atmospheric aerosols: composition, transformation, climate and health effects. Angew. Chem. Int. Ed. 44 (46), 7520–7540.

Saleh, R., Robinson, E.S., Tkacik, D.S., Ahern, A.T., Liu, S., Aiken, A.C., Sullivan, R.C., Presto, A.A., Dubey, M.K., Yokelson, R.J., Donahue, N.M., Robinson, A.L., 2014. Brownness of organics in aerosols from biomass burning linked to their black carbon content. Nat. Geosci. 7 (9), 647–650.

Song, J., He, L., Peng, P.a., Zhao, J., Ma, S., 2012. Chemical and isotopic composition of humic-like substances (HULIS) in ambient aerosols in Guangzhou, South China. Aerosol Sci. Technol. 46 (5), 533–546.

Srinivas, B., Rastogi, N., Sarin, M., Singh, A., Singh, D., 2016. Mass absorption efficiency of light absorbing organic aerosols from source region of paddy-residue burning emissions in the Indo-Gangetic Plain. Atmos. Environ. 125, 360–370.

Sun, J., Zhi, G., Hitzenberger, R., Chen, Y., Tian, C., Zhang, Y., Feng, Y., Cheng, M., Zhang, Y., Cai, J., 2017. Emission factors and light absorption properties of brown carbon from household coal combustion in China. Atmos. Chem. Phys. 17 (7), 4769–4780.

Szidat, S., 2009. Sources of Asian Haze. Science 5913, 470–471.

Szidat, S., Jenk, T.M., Gäggeler, H.W., Synal, H.-A., Fisseha, R., Baltensperger, U., Kalberer, M., Samburova, V., Wacker, L., Saurer, M., Schwikowski, M., Hajdas, I., 2004. Source apportionment of aerosols by 14C measurements in different carbonaceous particle fractions. Radiocarbon 46, 475–484.

Szidat, S., Prévôt, A.S.H., Sandradewi, J., Alfarra, M.R., Synal, H.-A., Wacker, L., Baltensperger, U., 2007. Dominant impact of residential wood burning on particulate matter in Alpine valleys during winter. Geophys. Res. Lett. 34, L05820.

Wang, J., Ho, S.S.H., Ma, S., Cao, J., Dai, W., Liu, S., Shen, Z., Huang, R., Wang, G., Han, Y., 2016. Characterization of PM2. 5 in Guangzhou, China: uses of organic markers for supporting source apportionment. Sci. Total Environ. 550, 961–971.

Washenfelder, R.A., Attwood, A.R., Brock, C.A., Guo, H., Xu, L., Weber, R.J., Ng, N.L., Allen, H.M., Ayres, B.R., Baumann, K., Cohen, R.C., Draper, D.C., Duffey, K.C., Edgerton, E., Fry, J.L., Hu, W.W., Jimenez, J.L., Palm, B.B., Romer, P., Stone, E.A., Wooldridge, P.J., Brown, S.S., 2015. Biomass burning dominates brown carbon absorption in the rural southeastern United States. Geophys. Res. Lett. 42, 653–664.

Weber, R., Sullivan, A., Peltier, R., Russell, A., Yan, B., Zheng, M., De Gouw, J., Warneke, C., Brock, C., Holloway, J., Atlas, E., Edgerton, E., 2007. A study of secondary organic aerosol formation in the anthropogenic-influenced southeastern United States. J. Geophys. Res.-Atmos. 112, D13302.

Winiger, P., Andersson, A., Eckhardt, S., Stohl, A., Gustafsson, Ö., 2016. The sources of atmospheric black carbon at a European gateway to the Arctic. Nat. Commun. 7, 12776.

Xie, M., Chen, X., Hays, M.D., Lewandowski, M., Offenberg, J., Kleindienst, T.E., Holder, A.L., 2017. Light Absorption of Secondary Organic Aerosol: Composition and Contribution of Nitroaromatic Compounds. Environ. Sci. Technol. 51 (20), 11607–11616.

Xu, X., Trumbore, S.E., Zheng, S., Southon, J.R., McDuffee, K.E., Luttgen, M., Liu, J.C., 2007. Modifying a sealed tube zinc reduction method for preparation of AMS graphite targets: reducing background and attaining high precision. Nucl. Instrum. Methods Phys. Res., Sect. B 259 (1), 320–329.

Yan, C., Zheng, M., Bosch, C., Andersson, A., Desyaterik, Y., Sullivan, A.P., Collett, J.L., Zhao, B., Wang, S., He, K., 2017. Important fossil source contribution to brown carbon in Beijing during winter. Sci. Rep. 7.

Yuan, J.-F., Huang, X.-F., Cao, L.-M., Cui, J., Zhu, Q., Huang, C.-N., Lan, Z.-J., He, L.-Y., 2016. Light absorption of brown carbon aerosol in the PRD region of China. Atmos. Chem. Phys. 16 (3), 1433–1443.

Zencak, Z., Elmquist, M., Gustafsson, Ö., 2007. Quantification and radiocarbon source apportionment of black carbon in atmospheric aerosols using the CTO-375 method. Atmos. Environ. 41, 7895–7906.

Zhang, X., Lin, Y.-H., Surratt, J.D., Weber, R.J., 2013. Sources, composition and absorption Ångstrom exponent of light-absorbing organic components in aerosol extracts from the Los Angeles Basin. Environ. Sci. Technol. 47 (8), 3685–3693.

Zhang, Y., Huang, R., El Haddad, I., Ho, K., Cao, J., Han, Y., Zotter, P., Bozzetti, C., Daellenbach, K., Canonaco, F., Slowik, J., Salazar, G., Schwikowski, M., Schnelle-Kreis, J., Abbaszade, G., Zimmermann, R., Baltensperger, U., Prévôt, A., Szidat, S., 2015. Fossil vs. non-fossil sources of fine carbonaceous aerosols in four Chinese cities during the extreme winter haze episode of 2013. Atmos. Chem. Phys. 15, 1299–1312.

Zotter, P., Ciobanu, V.G., Zhang, Y., El-Haddad, I., Macchia, M., Daellenbach, K.R., Salazar, G.A., Huang, R., Wacker, L., Hueglin, C., Piazzalunga, A., Fermo, P., Schwikowski, M., Baltensperger, U., Szidat, S., Prévôt, A.S.H., 2014. Radiocarbon analysis of elemental and organic carbon in Switzerland during winter-smog episodes from 2008 to 2012 - part 1: source apportionment and spatial variability. Atmos. Chem. Phys. 14, 13551–13570.